ELSEVIER

Ceramics International 29 (2003) 377–383

CERAMICS INTERNATIONAL

www.elsevier.com/locate/ceramint

Gehlenite and anorthite crystallisation from kaolinite and calcite mix

Karfa Traoré[a], Tibo Siméon Kabré[a], Philippe Blanchart[b,*]

[a]*Laboratoire de physico-chimie et de Technologie des Matériaux, UFR-SEA, Université de Ouagadougou, BP 7021 Ouagadougou 03, Burkina Faso*
[b]*GEMH, Ecole Nationale Superiure de Ceramique Industrielle (ENSCI), 48–73 Avenue Albert Thomas, Limoges 87065 cedex, France*

Received 11 April 2002; received in revised form 8 June 2002; accepted 28 June 2002

Abstract

Clay products can be reinforced by using clay and calcite mixes, even if sintering is at low temperature (1100 °C). The formation of a micro-composite microstructure favours a significant strength increase as fired materials contain anorthite grains embedded in a silico-aluminate matrix. The clay used, rich in kaolinite mineral, is originated from Burkina-Faso. It is contaminated by a moderate iron level, substituted to Al in octahedral sites of kaolinite, influencing the thermal comportment. An alternative approach was also used when substituting the common clay by an almost pure kaolinite mineral, to understand the iron role. In general, during thermal transformations, the reaction sequence of recrystallisation is metakaolinite—gehlenite—anorthite, but mullite was never detected. The interpretations of DTA spectrums indicate increasing activation energy for gehlenite and then anorthite formations. For mullite, although the corresponding activation energy is the lowest, it is not present. This energetically interpretation differs from the analysis of the SiO_2–Al_2O_3–CaO ternary diagram, where transformation paths are not so clear. It is then proposed that the reaction sequence is favoured by the existence of structural similarities between metakaolinite, gehlenite and anorthite, which are pseudo-layered structures. For mullite, the 3D structure is very different, which explains its absence in the material.

Keywords: A. Sintering; B. Composites; D. Clays; Anorthite

1. Introduction

Mineral raw materials are extensively used for more or less complex ceramic compositions since times in a large range of possible applications. Particularly, structural clay products composed of common clays and more complex refractory materials are currently produced. For many materials, the ceramic process results in significant strains, which must be controlled to attain a high quality level. For example, the controlled densification during a rapid firing or the accurate shape control during a liquid phase sintering are encountered difficulties.

These particular characteristics of ceramic materials are often affected by the existence of micro-composite microstructures with a crystalline phase embedded in a silico-alumina matrix. Phase dispersion and size, as the grain shape influence the whole material properties. Particularly, it is the case of the mullite phase in porcelain or refractory. In general, a very specific characteristic of these particulate composite materials is the reaction sintering process with more or less liquid phase and the nucleation and growth of new crystalline phases.

In the area of mineral raw materials, we must consider firstly clays and clay minerals, mainly kaolinite. This mineral is often used, for its adequate properties and because it enters in the mineralogical composition of many suitable clays for ceramics.

In this study, we used a common kaolinitic clay from Burkina Faso, which contains a moderate iron level. It is mixed with calcite to obtain particular structural transformation of the material during sintering, to obtain a micro-composite microstructure at the micron scale (Fig. 1) during sintering at a relatively low temperature (1100 °C). The anorthite particulate phase is tri-dimensionally dispersed in a silico-aluminate matrix, resulting in a significantly increase of mechanical

* Corresponding author. Tel.: +33-555-45-22-22; fax; +33-5-55-79-09-98.
E-mail address: p.blanchart@ensci.fr (P. Blanchart).

0272-8842/02/$22.00
PII: S0272-8842(02)00148-7

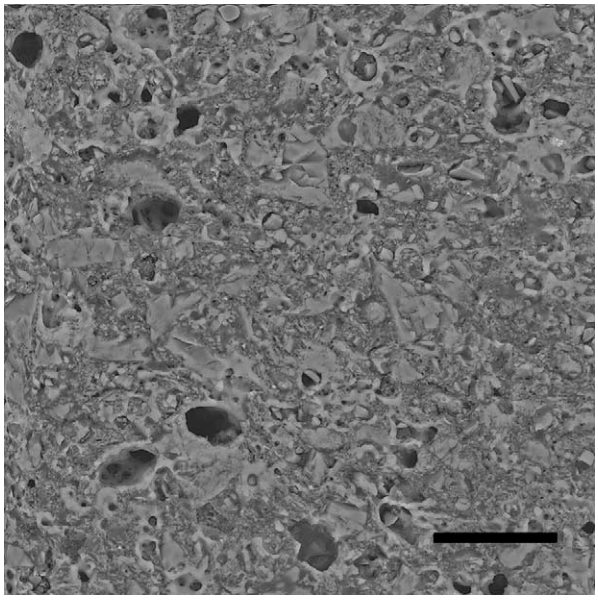

Fig. 1. Scanning electronic microscopy of the P2 material sintered at 1100 °C, 1 h. Bar = 15 μm.

strength. Results from this common clay were compared to that from pure kaolinite with a low impurity level.

2. Materials and methods

P1 clay chemical and mineralogical compositions are in Tables 1 and 2, respectively [1]. The major mineral species are kaolinite and quartz, but minor minerals quantities were not detected by X-ray. Nevertheless, the major impurity is iron and its environment was more precisely examined by Mössbauer spectroscopy as the detection level of this method is low and it proved to be useful in the case of clay and kaolins.

In kaolinite mineral, structural Al can be partially substituted by Fe. From Mössbauer investigations, the presence of octahedrally co-ordinated Fe^{III} was well established [2]. There is also Fe^{II}, substituted trioctahedrally in the structure [3–5]. Detailed, parameters of Mössbauer spectra, corresponding to Fe^{III} in kaolinite tetrahedral sites were published in Petit and Decarreau [6]. Iron can be also detected under the form of various iron species [7], but the most widely occurring Fe oxides are hematite, mostly as very fine particles [8] or goethite, adsorbed on kaolinite surfaces [9].

For P1, the experimental Mössbauer spectrum (Fig. 2) was simulated by two typical doublets, a very large one associated to a small one. The former is related to octahedral Fe^{III} (Isomer shift = 0.37 mm/s; Quadrupole splitting S = 0.59 mm/s; Line width = 0.54) [6], in quantity of 94.5%. The small doublet (5.5%) corresponds to Fe^{II} also in octahedral sites (Isomer shift = 1.17 mm/s; Quadrupole splitting S = 2.2 mm/s ; Line width = 0.54) [4]. A similar spectrum was soon observed with pure kaolinitic clays [5], but in P1 no added response from a possible iron mineral was detected.

Apart P1 clay, the reference mineral is the KGa-2 from the Clay Mineral Society (Missouri University). It is a poorly crystallised mineral containing at least 97% of kaolinite and a very reduced impurity level (Tables 1 and 2). The reference character of KGa-2 was checked by the comparison of the cristallinity degree of P1 and KGa-2 kaolinite minerals by X-rays. We measured the broadening of [00l] diffraction peaks and from respective heights of the [110] and [111] peak (Fig. 3). Taking account the similarity of X-Ray patterns from P1 finer fraction and KGa-2 clay, we referenced the P1 composition by KGa-2 mixed with quartz, in a size range similar to that of P1. It is then possible to examine the iron influence on the P1 thermal comportment.

Mixed ceramic paste compositions are indicated in Table 3. For calcium addition, we used a calcite powder, in a granulometry range similar to that of quartz. P1 is the original paste containing only this raw material. P2 is the improved composition by adding 15 wt.% of calcite. M2 is a mix of reference minerals similar to P2 mineralogical composition. All compositions were grounded (90 wt.% < 8 μm) with an alumina jar and alumina balls during 1 h in water, dried, granulated and

Table 1
Global chemical analysis of crude P1 clay and KGa-2 kaolinite

Wt.%	P1	KGa-2
Al_2O_3	28.20	38.5
Fe_2O_3	4.48	1.1
Na_2O	0.06	< 0.005
K_2O	0.72	0.065
SiO_2	54.30	43.9
CaO	0.01	–
MgO	0.33	0.03
TiO_2	1.37	2.08
Loss	11.10	13.77

Table 2
Mineralogical compositions of P1 clay and KGa-2 reference kaolin

	P1	KGa-2
Kaolinite	71.4 ± 1	97
Quartz	21.1 ± 1	< 1
Rutile	–	2.1
Organic matter	7.5 ± 1	–

Table 3
Ceramic paste compositions

Paste compositions (wt.%)	P1	KGa-2	Quartz	Calcite
P1	100	0	0	0
P2	85	0	0	15
M2	0	64.2	20.8	15

die pressed. Material sintering was realised at 1100 °C, 1 h, with a 3 °C/min heating rate.

Thermal transformations were investigated by DSC (Setaram, Multi HTC), under air atmosphere.

3. Results

Fig. 1 presents a back scattered SEM image of P2 sample sintered at 1100 °C, 1 h (Hitachi S2500). We observe dense crystallised grains dispersed in a fine-grained porous matrix. Dense grains are very big compared to the matrix components and various medium to large sized pores are also seen.

X-rays from this material indicates clearly a predominant anorthite phase and quartz, but also a small amount of a calcium aluminium silicate phase, most probably an anorthite poly-type phase. The material appears to be composed of dense anorthite grains into a poorly crystallised and heterogeneous matrix.

The morphology and repartition of the anorthite dispersed phase were observed by image analysis of a SEM image (Fig. 1), using classical morphological tools (Fig. 4). It is seen that dense grains are distributed throughout the matrix phase to form an interconnected network. It contributes to the material strength although pores are essentially located into the matrix phase.

A correlation is also found when some dense anorthite grains occur near large pores. They are originated from calcite decarbonatation during the thermal cycle, leading to local calcium higher concentration which favours the in situ anorthite formation.

DSC analysis of M2, at different heating rates in the range 1, 2, 3 and 5°/min, highlight a significant peak splitting below 5°/min (Fig. 5). For the lower heating rates, it can be assumed that the process proceeds slowly comparatively to the calorimeter time constant. Since 5 °C/min and above, additional phenomena contribute to the non-isothermal approach and thermal gradient in the sample cannot be effectively corrected. Otherwise, a particle size effect and strains induced by reactant disintegration modified the idealised representation of a powder compact where an advancing interface can progress from one nucleated particle to a neighbouring unreacted one. The material heterogeneity, at the grain size dimension, should be taken into consideration.

For M2, heated at 1, 2 and 3 °C/min, we report peak temperatures and heath flows from the DSC signal (Fig. 5 and Table 4). When the heating rate increases, the two peaks are shifted towards the higher temperature whether peak distances remain almost constant.

Heat flows from DSC are connected to the fractional reaction α. They are connected by the following relation [10], arranged in the case of DSC:

$$\frac{d\alpha}{dt} = \frac{dH}{dt}(S - s) \quad (1)$$

where H is the enthalpy, S is the peak surface between the lower and upper bounds and s is the fractional peak surface between the lower bound and t°C. Problems arise from the S evaluation, since peak bounds cannot be precisely obtained for complex materials, when the curve background is curvilinear. Nevertheless, for M2, two well-separated peaks indicate the completion of two successive transformations. Respective transformation heaths for the lower and the higher temperature peaks vary slightly with the heating rate used (Table 4). It supports a very low dependence from the heating rate of the mechanism involved in transformations and therefore on the kinetic model used. Kinetic measurements can be therefore taken on the experimental curves without correction.

For P2, the large DSC peak (Fig. 6) is obviously a complex peak from at least two overlapped peaks. Although it is not possible to obtain an accurate peak deconvolution, a significant shift of peak temperature is observed as the heating rate increases. Nevertheless, the

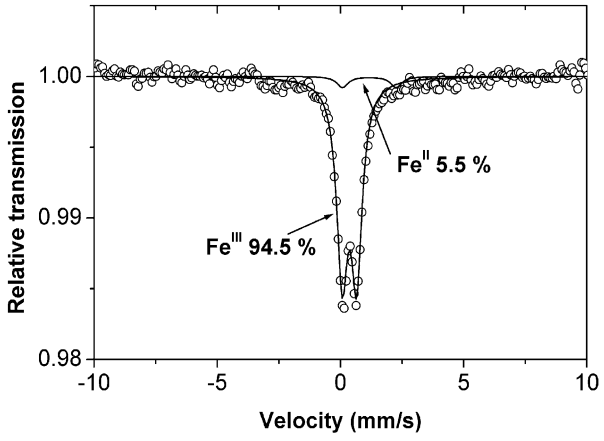

Fig. 2. Mössbauer spectra of P1 clay. Experimental data points and simulation by two doublets.

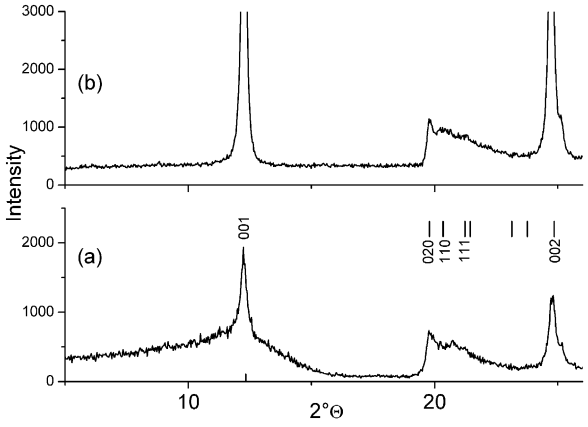

Fig. 3. X-ray spectrum of (a) P1 finer fraction (<2 μm); (b) KGa-2 kaolin.

global heat flows appears to be equivalent to that obtained with M2, which means that the whole processes should be similar in nature but somewhat different as regards kinetics.

4. Discussion

The composite microstructure origin can be firstly examined considering the formation of crystalline phases. X-ray analysis of materials at temperatures before, between and above the two peaks indicated the occurrence of well-known phases. Firstly, the gehlenite intermediate phase is crystallised from metakaolinite and calcium, under the reaction [11]:

$$Al_2Si_2O7 + (2 + n)CaO \rightarrow Ca_2Al_2SiO7 + nCaOSiO_2 \quad (2)$$

This reaction should involve the formation of calcium compounds, in accordance with the ternary diagram SiO_2–Al_2O_3–CaO [12]. Beside gehlenite, any occurrence of minor phases was observed, excepted quartz from the starting composition.

The second reaction step is the anorthite formation from gehlenite, which is combined with aluminium and silicon from metakaolinite and the remaining fine quartz:

$$Ca_2Al_2SiO_7 + 3SiO_2 + Al_2O_3 \rightarrow 2CaAl_2Si_2O_8 \quad (3)$$

From the global chemical composition (Table 3), the maximum anorthite content can be calculated, 42 wt.%, if all Ca atoms are combined. Nevertheless, the powder mixing process leads to heterogeneity at the grain scale and only 25–30 wt.% of anorthite was detected by X-rays. Anorthite should be crystallised since the local calcium quantity exceed a sufficient level. It means that the matrix material is composed of reduced quantity of calcium aluminium silicate phases, heterogeneously distributed and associated with quartz, possible iron phases and pores.

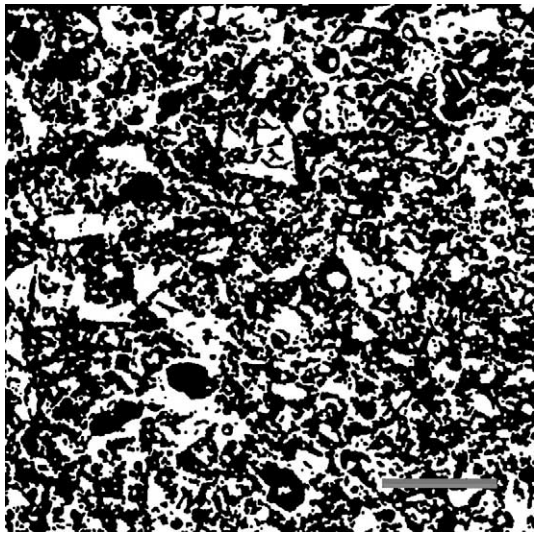

Fig. 4. Image analysis of SEM image of Fig. 1. The white anorthite phase is distributed into the dark matrix. Bar = 15 μm.

Besides calcium compounds, mullite was never detected by X-ray diffraction. This particularity must be linked to the ternary diagram SiO_2–Al_2O_3–CaO (Fig. 7), were the P2 and M2 composition points are reported. Although phase diagram apply only to equilibrium, it is noted that our global composition points are closed to the anorthite area, but in the mullite and silica zone. The low sintering temperature of our material is far below possible liquid temperatures (L point at 1345 °C and N point at 1380 °C), indicating the existence of dominant solid phase mechanisms. It is also supported by pseudo-binary diagrams: anorthite–alumina [13]; Anorthite–silica [14]; Anorthite–gehlenite [15]. They only state at 1100 °C the possible co-existence of solid phases without any solid solutions. It can be suggested therefore that the early gehlenite crystallisation is a first step related to easy calcium diffusion throughout the heterogeneous material. In a second step, anorthite, mullite and silica (cristobalite) should co-exist. Here we suggest the effect of the low sintering temperature which limit the extend of the matrix structural reorganisation.

A different possible approach to phase formation uses a kinetic interpretation of thermal analysis. For non-isothermal experiments, temperature is related to the reaction rate through the Arrhenius equation [16]:

$$\frac{d\alpha}{dt} = \left(\frac{A}{\beta}\right)\exp\left(-\frac{E_a}{RT}\right)f(\alpha) \quad (4)$$

α is the fractional reaction, β the heating rate, T the temperature and R the gas constant. The kinetic parameters E_a and A are the energy barrier to reaction and the frequency of occurrence of the phenomena. It may lead to compare reactivities of different systems. $f(\alpha)$ is a kinetic expression which take into account reaction mechanisms.

Table 4
Transformation heats and T_{max} values for gehlenite and anorthite from M2

	Transformation heats (J/g)		T_{max} (°C)	
	Gehlenite	Anorthite	Gehlenite	Anorthite
1 °C/min	19±1	38±1	933	954
2 °C/min	20±1	39±1	945	965
3 °C/min	22±1	42±1	955	973

For non-isothermal analyses, the assumption of the kinetic model $f(\alpha)$ is preliminary made, most generally as a n' order reaction model ($f(\alpha)=(1\text{-}\alpha)^n$). Although extensive discussion has been made in literature about this a priori choice, experimental results of parameters are generally comparable to that obtained with isothermal methods.

To estimate kinetic parameters, a useful approach involves the use of the second derivative of Eq. (4) with respect to temperature. This derivative is zero at the maximum of the DSC peak, when T attains T_{max} for the peak considered.

This method was used by Kissinger [17] and generalised afterwards [18] to make it applicable to a large range of kinetic models. The second derivative of eq. (4), when $f(\alpha)$ is a n' order reaction is:

$$\ln\left(\frac{\beta}{T_{max}^2}\right)=\ln\left(\frac{A\mathrm{R}}{E_a}\right)+\ln(n(1-\alpha_{max})^n)-\frac{E_a}{\mathrm{R}T_{max}} \quad (5)$$

where T_{max} is the maximum peak temperature. The influence of n appears to be small since α_{max} tends to 1 at the completion of the reaction. The E_a value is obtained from a plot of $\ln(\beta_i/T_{max}^2)$ against $1/T_{max}$ for a series of experiments at different heating rates β_i.

From experimental data of T_{max} (Table 4), Kissinger plots are in Fig. 8 for gehlenite and anorthite of M2. The E_a value is 604 kJ/mol for gehlenite and 743 kJ/mol for anorthite. For P2, only an E_a evaluation could be made, at slightly lower values than that for M2. Here the structural iron role of P1 is pointed out. It favours the structural transformation of metakolinite to gehlenite and anorthite. This point can be connected to iron environment study in kaolinite, as a function of temperature. It was shown that the structural iron from kaolinite (Fe^{III}) can be more easily displaced from its initial environment, leading to structural distortions and vacancies [4].

For mullite, which should crystallize in P1, the E_a value is 420 kJ/mol, i.e. in the data range, 210–840 kJ/mol, obtained with number of mullite from different sources [19,20]. Under the earlier results, some mullite should be detected in the matrix phase.

To explain the reaction sequence of metakaolinite to gehlenite and then anorthite, we also consider structural similarities between these phases whereas mullite structure is very different. Above dehydroxylation (650 °C), metakaolinite is a single layer structure [21] where Si are tetrahedraly coordinated, as in the kaolinite (Fig. 9), although a limited ordering of tetrahedras is supposed in the [110] plane. Al are four-fold coordinated, in a very disordered environment and restore progressively a six-fold coordination above 900 °C [22].

The gehlenite structure [23] is similar to a single layer structure parallel to [001] (Fig. 10). It consists of sheets where 1/2Al + 1/2Si are in distorted tetrahedras, linked at one corner in pairs. Al bringing atoms in AlO_4 tetrahedras are situated at corners and centre of the base. Ca atoms lie between these sheets within distorted oxygen square antiprisms.

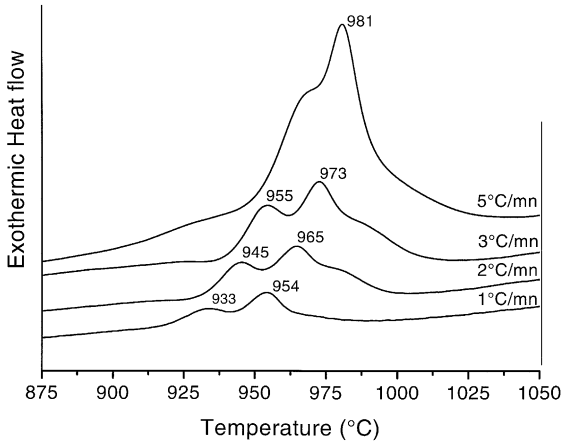

Fig. 5. DSC analysis of M2 sample at 1, 2, 3 and 5°/min heating rates.

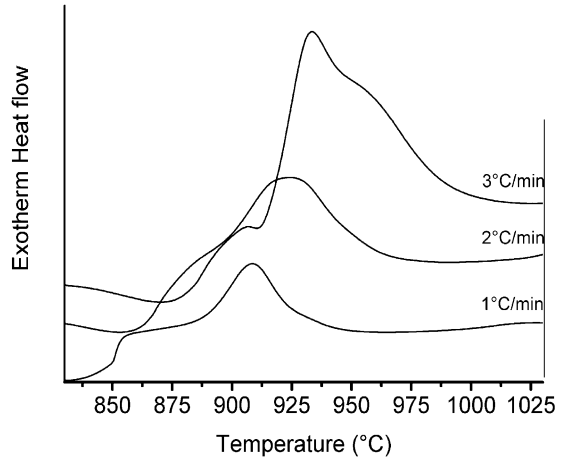

Fig. 6. DSC analysis of P2 sample at 1, 2 and 3°/min heating rates.

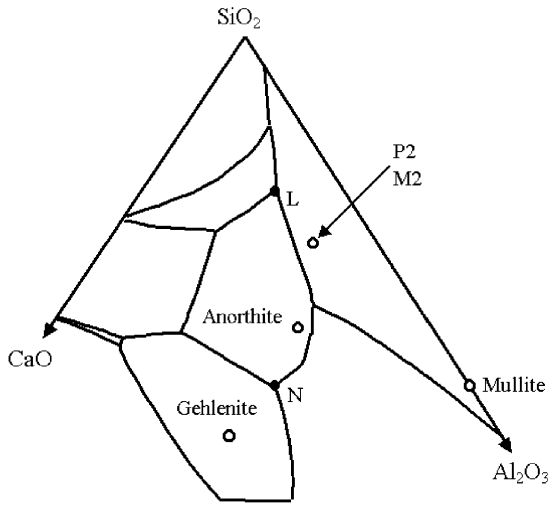

Fig. 7. Silica rich part of the ternary diagram SiO_2–Al_2O_3–CaO [12].

The basic idea is the similarities between metakaolinite and gehlenite structures. Particularly, the occurrence of the same type of tetrahedras containing sheets suggest a topotactical transformation. This hypothesis is supported by the generally accepted statement that showed the conservation of SiO_4 tetrahedras in metakaolinite through the thermal process, whereas the AlO_6 structures units decompose during dehydroxylation, to form four-fold distorted environments.

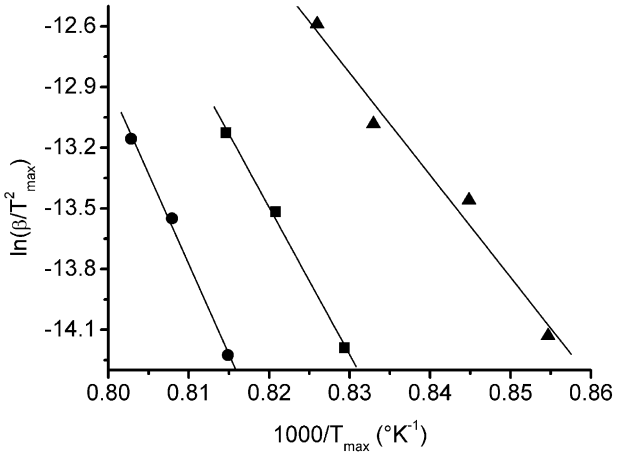

Fig. 8. Kisinger plots for gehlenite (square) and anorthite (circle) in M2 and for mullite (triangle) in P1.

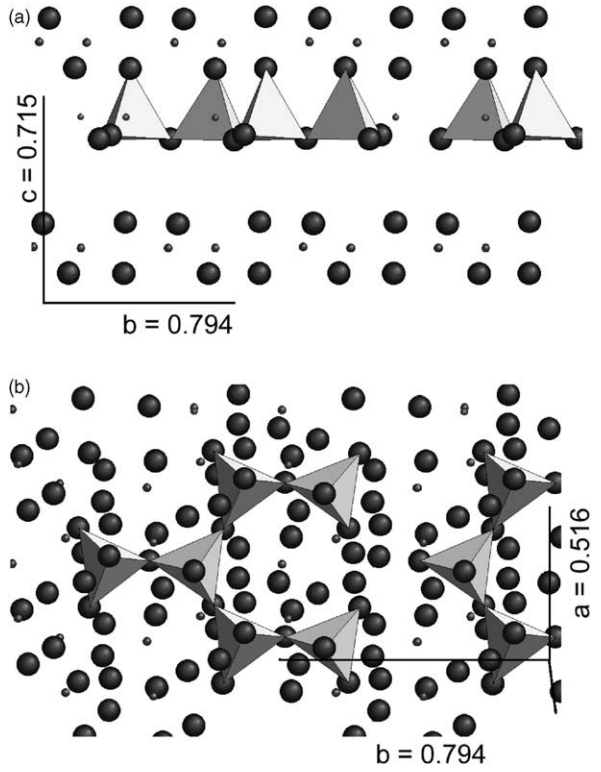

Fig. 9. Aspect of Metakaolinite structure (nm scale). (a) [110]; (b) [001].

The Si and Al units in metakaolinite, parallel to the [110] direction, seem to collapse in more compact layers of gehlenite (Fig. 9). They contain Al in isolated tetrahedras and pairs of Al and Si distorted tetrahedras. Ca cations are in interlayer position where they compensate for the weak charges of the composite layers. They are very weakly bounded and they can easily diffuse along the layer direction.

For anorthite, it is a double sheet silicate, also in the [110] direction with a monoclinic symmetry and a characteristic double c value (14.169 Å) [24]. It is char-

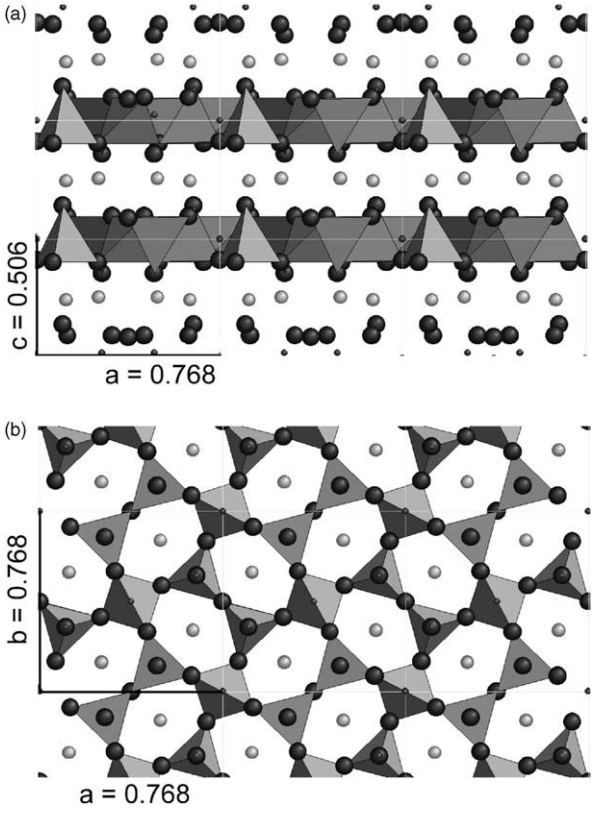

Fig. 10. Aspect of Gehlenite structure (nm scale). (a) [110]; (b) [001].

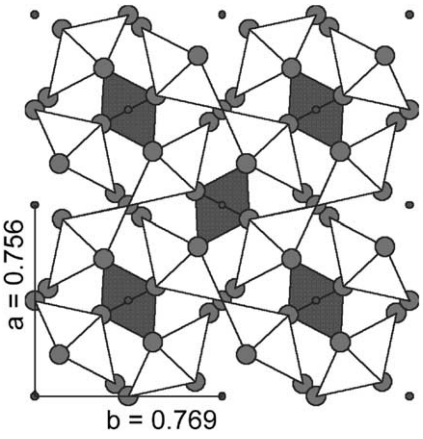

Fig. 11. [001] Projection of mullite structure. Projection of octahedral columns (dark) are linked by tetrahedras. Cell parameters are in nm.

acterised by particular ordered chains of tetrahedras units along the large *a* and *b* values (8.177 and 12.877 Ă).

Unlike these structures, mullite is very different [25] as its average structure contains columns of edge-sharing octaedras, with Al, that form chains running parallel to the *c* axis (Fig. 11). They are cross linked by tetrahedra chains along the *c* axis, with Si and Al ions. In this double chain structure, octahedral chains are firmly built.

5. Conclusion

The formation of a micro-composite microstructure from a sintered kaolinite clay and calcite mix is originated from the preferential reaction sequence metakaolinite–gehlenite–anorthite. It is favoured by increased activation energies of transformations although the comparison with the transformation path of an ideal mix in equilibrium, in the ternary phase diagram SiO_2–Al_2O_3–CaO suggest a different path. Reactions are also provoked by the existence of structural similarities of layered structures of metakolinite, gehlenite and anorthite. The presence of structural iron in Al octahedral sites of kaolinite increases the reaction kinetics. For mullite, the large difference in nature of the 3D structure explains its absence although the energetically aspect and the phase diagram interpretation.

Acknowledgements

Authors grateful acknowledge the AIRE-Development and the IRD French agencies for long time support of research and development in the Ouagadougou University. We would like to thank the French government foreign office for also supporting this work under the PAE-Sup Burkina Faso program.

References

[1] K. Traoré, T.S. Kabré, P. Blanchart, Sintering of a clay from Burkina Faso by dilatometry. Influence of the applied load and the pre-sinteringheating rate, Ceram. Int. 27 (2001) 875–882.
[2] P.J. Malden, R.E. Meads, Substitution by iron in kaolinite, Nature 215 (1967) 844–846.
[3] D.A. Jefferson, M.J. Tricker, A.P. Winterbottom, Electron microscopy and Mössbauer spectroscopic studies of iron-stained kaolinite minerals, Clays and Clay Minerals 23 (1975) 355–360.
[4] E. Murad, U. Wagner, Mössbauer spectra of kaolinite, halloysite and the firing products of kaolinite, N. Jahrb. Miner. 162 (1991) 281–309.
[5] A.H. Cuttler, The behaviour of a synthetic 57Fe doped kaolin: Mössbauer and electron paramagnetic resonance studies, Clay Miner. 15 (1980) 429–444.
[6] S. Petit, A. Decarreau, Hydrothermal synthesis and crystal chemistry of iron-rich kaolinites, Clay Miner. 25 (1990) 181–196.
[7] C.S. Hogg, P.J. Malden, R.E. Meads, Identification of iron containing impurities in naturral kaolinites using the Mössbauer spectroscopy effect, Min. Mag. 40 (1975) 89–96.
[8] C. Janot, H. Gibert, C. Tobias, Caracterisation de kaolinites ferrifères par spectroscopie Mösbauer, Bull. Soc. Fr. Mineral. Cristallogr. 96 (1973) 281–291.
[9] S.A. Fysh, P.E. Clark, Aluminous Goethite, a Mössbauer study, Phys. Chem. Minerals 8 (1982) 180–187.
[10] E. Koch, B. Stikerieg, DTA curves and non isothermal reaction rates, Thermochim. Acta 17 (1976) 1–16.
[11] K. Traoré, T.S. Kabré, P. Blanchart, Low temperature sintering of a clay for pottery from Burkina Faso, Appl. Clay Sci. 17 (5) (2000) 279–292.
[12] E.F. Osborn, A. Muan, System SiO_2–CaO–Al_2O_3. Phase equilibrium diagrams of oxide systems, Fig. 630, 1960, Am. Ceram. Soc.
[13] G.A. Rankin, F.E. Wright, System α–Al_2O_3–CaO.Al_2O_3.2SiO_2, Am. J. Sci., 4th Ser. 39 (1915) 47.
[14] O. Andersen, System SiO_2–CaO.Al_2O_3.2SiO_2, Am. J. Sci., 4th Ser. 39 (1915) 423.
[15] G.A. Rankin, F.E. Wright, System CaO.Al_2O_3.SiO_2–CaO.Al_2O_3.2SiO_2, Am. J. Sci., 4th Ser. 39 (1915) 49.
[16] A.K. Galwey, M.E. Brown, Kinetic background to thermal analysis and calorimetry, Handbook of Thermal Analysis and Calorimetry 1 (1998) 147–217.
[17] H.E. Kissinger, Reaction kinetics in differential thermal analysis, Anal. Chem. 29 (1957) 1702–1706.
[18] J.P.J. Elder, Thermal Anal. 30 (1985) 657.
[19] D. Prodanovic, Z.B. Zivkovic, S. Radosavljivic, Kinetics of the dehydroxylation and mullitization processes of the halloysite from the Farbani Potok locality, Serbia, Appl. Clay Sci. 12 (1997) 267–274.
[20] T. Takei, Y. Kameshima, A. Yasumori, K. Okada, Crystallization kinetics of mullite from Al_2O_3–SiO_2 glasses under non-isothermal conditions, J. Eur. Ceram. Soc. 21 (2001) 2487–2493.
[21] A. Gualtieri, M. Belloto, Modelling the structure of the metastable phases in the reaction sequence kaolinite–mullite by X-ray scattering experiments, Phys. Chem. Minerals 21 (1994) 442–452.
[22] J. Sanz, A. Madani, J.M. Serratosa, J.S. Moya, S. Aza, Aluminum and silica magic angle spinning nuclear magnetic resonance study of the kaolinite–mullite transformation, J. Am. Ceram. Soc. 71 (1998) 418–421.
[23] S. Thayaparam, M.T. Dove, V. Heine, A computer simulation study of Al/Si ordering in gehlenite and the paradox of the low transition temperature, Phys. Chem. Minerals 21 (1994) 110–116.
[24] L.S. Bragg, G.F. Claringbull, W.H. Taylor, Crystal structures of minerals, The Crystalline State vol. IV (1965) 304–339.
[25] J.A. Ross, C.T. Prewitt, Cystal structure of mullite: a re-examination of the average structure, Am. Miner. 71 (1986) 1476–1482.